PLEASE CITE THIS ARTICLE AS DOI: 10.1063/1.5057424

1

20

21

22

2 J. Occena, T. Jen, J. W. Mitchell, W. M. Linhart, E.-M. Pavelescu, R. Kudrawiec, Y. Q. 3 Wang,4 R. S. Goldman1* 4 ¹Department of Materials Science and Engineering, University of Michigan, Ann Arbor, 5 Michigan 48109-2136, USA 6 ² Faculty of Fundamental Problems of Technology, Wrocław University of Science and 7 Technology, 50-370 Wrocław, Poland 8 ³ National Institute for Research and Development in Microtechnologies, 077190 Bucharest, 9 Romania 10 ⁴ Materials Science and Technology Division, Los Alamos National Laboratory, Los 11 Alamos, New Mexico 87545, USA 12 July 19, 2019(b) 13 14 **ABSTRACT** 15 We have examined the alloy composition dependence of the energy bandgap and electronic 16 states in GaAsNBi alloys. Using direct measurements of N and Bi mole fractions, via ion beam 17 analysis, in conjunction with direct measurements of the out-of-plane misfit via x-ray rocking 18 curves, we determine the "magic ratio" for lattice-matching of GaAsNBi alloys with GaAs 19 In addition, using a combination of photoreflectance and photoluminescence substrates.

spectroscopy, we map the composition- and misfit-dependence of the energy bandgaps, along with

revealing the energetic position of Bi-related states at approximately 0.18 eV above the valence

Mapping the composition-dependence of the energy bandgap of GaAsNBi alloys

23 *Corresponding Author: <u>rsgold@umich.edu</u>

band maximum.

This is the author's peer reviewed, accepted manuscript. However, the online version of record will be different from this version once it has been copyedited and typeset PLEASE CITE THIS ARTICLE AS DOI: 10.1063/1.5057424

Due to the significant bandgap narrowing induced by the incorporation of dilute fractions of N and Bi in compound semiconductors, emerging dilute nitride-bismide alloys are of significant interest for optoelectronic devices operating in the near- to mid-infrared range. In the literature, the magic N to Bi mole fraction ratio for lattice matching of GaAsNBi with GaAs is predicted to be equal to 0.59, based upon a computed value of the GaBi lattice parameter. In addition, the relationship between the composition and the bandgap value is most often determined using x-ray diffraction measurements of strain to determine the alloy composition, assuming the computed value of the GaBi lattice parameter, with films fully strained to the GaAs substrate. For GaAsNBi, it has recently been shown that Bi promotes the formation of (N-As)_{As} interstitial complexes, which are not accounted for in typical analyses of x-ray diffraction data. Furthermore, it has been proposed that Bi behaves as an isoelectronic impurity in GaAs. However, there are conflicting reports regarding the energetic position of the Bi impurity state either 0.18 eV above or 0.08 – 0.4 eV below^{4,5,6,7,8,9} the valence band maximum.

Here, we use a combination of direct measurements of alloy compositions, via ion beam analyses of the N and Bi mole fractions, in conjunction with direct measurements of the out-of-plane misfit using high-resolution x-ray diffraction and measurements of bandgap using photoreflectance (PR), to determine a N/Bi ratio for lattice-matching and a map of the composition dependence of GaAsNBi bandgaps. Furthermore, a comparison of photoreflectance and photoluminescence spectra reveals the presence of a Bi-related state ~0.18 eV above the valence band edge, consistent with the predictions of Janotti et al. These findings offer a predictive guide to bandgap engineering using GaAsNBi alloys and provide insight into the combined influence of Bi and N on electronic structure that may be extended to other emerging dilute nitride-bismide alloys, such as GaPNBi and InAsNBi.

PLEASE CITE THIS ARTICLE AS DOI: 10.1063/1.5057424

A series of GaAs_{1-x-y}N_xBi_y films were grown by molecular-beam epitaxy, as described elsewhere.^{3,10} A range of N and Bi fractions were achieved by varying the N₂ flow rate from 0 to 0.35 sccm (N flux series) and the Bi beam-equivalent pressure (BEP) from 0 to 1.2×10^{-7} Torr (Bi flux series). Films with 100nm ("thin") and 400nm ("thick") thicknesses were prepared. High-resolution x-ray diffraction measurements were performed using a Bede D1 and/or Rigaku Smartlab diffractometer with CuKa1 radiation using radiation monochromated by two Si channel cut crystals, consisting of (220) reflections in the duMond-Hart-Bartels (+,-,-,+) configuration. X-ray rocking curves (XRCs) were collected near the (004) and (224) GaAs reflections. They out-of-plane misfit was determined directly from the (004) XRCs as:

$$\varepsilon_{\perp} = \frac{\sin(\theta_B)}{\sin(\theta_B + \Delta\omega)} - 1 \tag{1}$$

where θ_B is the Bragg angle for GaAs for the (004) reflection and $\Delta\omega$ is the peak splitting between the film and the GaAs substrate for the (004) reflection. The in-plane misfit was determined from an analysis of glancing-incidence (224) XRCs; the misfit and residual in-plane strain were then computed assuming a tetragonally distorted lattice with the Poisson ratio of GaAs, as described in the Supplementary Materials. The resulting misfit values range from -0.16% to 0.46%. According to Refs. 12,13,14, the critical thickness for dislocation nucleation is expected to exceed 200 nm. Thus, the "thin" films are expected to be coherently strained, consistent with the negligible strain relaxation computed using XRC, as shown in Table S1 of the supplementary materials. For the "thick" films which contain Bi, negligible strain relaxation is also observed, suggesting that they are also coherently strained. However, the "thick" film without Bi is partially (14%) relaxed, presumably due to the nucleation of 90° partial dislocations whose misfit component is nearly double that of 60° dislocations. Indeed, 90° partial dislocations have been observed in tensile-strained films such as GaAsN. If the attribute the (004) XRC linewidths for

PLEASE CITE THIS ARTICLE AS DOI: 10.1063/1.5057424

1

2 "thick" film (60 arcseconds) to 90° partial dislocations, the resulting dislocation densities would 3 be \sim 5 x 10⁵/cm² and 2 x 10⁶/cm², consistent with the differences in measured strain relaxation. In this case, the lack of appreciable strain relaxation in the Bi-containing tensile strained "thick" film 4 is likely due to the surfactant action of Bi suppressing the formation of 90° partial dislocations. 5 6 For all films, the Bi fractions were determined using Rutherford backscattering 7 spectrometry (RBS), in conjunction with simulation of nuclear reaction analysis (SIMNRA) code, 8 as described elsewhere.^{3,17} For the thin films, the total, substitutional, and interstitial N fractions 9 were determined using channeling nuclear reaction analysis (NRA), also in conjunction with 10 SIMNRA code. In addition, for all films, the Bi fractions from RBS and the nominal film 11 thicknesses were used as input into dynamical diffraction simulations via the Rocking-Curve 12 Analysis by Dynamical Simulations (RADS) software. Interestingly, the RADS-determined N 13 fractions were consistent with the substitional N fraction determined using NRA, which is typically 75% of the total N fraction determined using NRA, consistent with trends reported elsewhere.^{3,15} 14 15 Therefore, to take into account the interstitials in the thick films, the total N fraction was determined as the RADS N fraction (substitutional fraction) divided by 0.75.3,18 16 17 To measure the photoreflectance (PR) spectra, each sample was mounted on a cold finger 18 in a helium closed cycle refrigerator coupled with a programmable temperature controller, 19 allowing measurements in the 20 - 320 K temperature range. The reflected light from the sample 20 was dispersed by a single grating 0.55 m focal-length monochromator and detected using a 21 thermoelectrically cooled InGaAs p-i-n photodiode. To illuminate the sample, a semiconductor 22 laser (532 nm line) and a 150 W tungsten-halogen bulb were used as the pump and probe beams, 23 respectively, which were focused onto the sample to a diameter of ~2 mm. The pump beam was

the Bi-containing "thick" films (52.5 \pm 2.5 arcseconds) to 60° dislocations and that of the Bi-free

PLEASE CITE THIS ARTICLE AS DOI: 10.1063/1.5057424

modulated by a mechanical chopper at a frequency of 290 Hz. Phase sensitive detection of the PR signal was made using a lock-in amplifier. Photoluminescence (PL) spectra were collected using a continuous-wave laser with wavelength of 532 nm and excitation powers of 100 or 300 mW.

In Fig. 1, contours of out-of-plane misfit are presented on a plot of Bi vs. N fraction for

GaAs_{1-x-y}N_xBi_y films with circular and square symbols correspond to 100nm and 400 nm thick films, respectively. For each composition, the out-of-plane misfit, ϵ_{\perp} , determined from (004) x-ray rocking curves, as described in Eqn. (1) above, is labeled near each point. Using a planar fit to the data points represented by circular symbols, with R² = 0.97, contours of constant ϵ_{\perp} , indicated by dashed black lines, reveal a N to Bi mole fraction ratio for lattice-matching of 0.83. For comparison, the predicted lattice-matched N to Bi mole fraction ratios of 0.59 from Janotti et al.¹ and 0.49 estimated using x-ray diffraction determinations of the N fraction by Huang et al.,¹⁹ are shown by gray lines. We note that a non-negligible fraction of the N in GaAsNBi has been reported to be incorporated interstitially,^{3,20} predominantly in the form of (N-As)_{As} complexes, which are not accounted for in Janotti's calculations and the x-ray diffraction determinations of N fraction by Huang et al.¹⁹ and Tixier et al.²¹ Indeed, a planar fit to ϵ_{\perp} , using the substitutional N fraction, rather than the total N fraction, yields a lattice-matched N to Bi mole fraction ratio of 0.61, in agreement with the predictions of Janotti et al.¹

We now consider the optical properties of the N flux series and Bi flux series of GaAsNBi alloys, as shown in the low-temperature (i.e. T = 20 K) PR spectra shown in Figs. 2(a) and 2(b), respectively. For each PR spectrum, features that are attributed to energy transitions, i.e. resonances, are apparent. To determine the energy, E_0 , of each transition and its broadening, the PR spectra were fitted using the Aspnes Formula:²²

23
$$\frac{dR}{R}(E) = \text{Re}\left[Ce^{i\vartheta}(E - E_0 + i\Gamma)^{-m}\right],\tag{2}$$

- where $\frac{dR}{R}(E)$ is the energy dependence of the PR signal, C and θ denote the amplitude and phase,
- 2 and E_0 and Γ are the energy and the broadening parameter of the optical transition, respectively.
- 3 Assuming m = 2 for an excitonic transition, we fit each spectrum with a low and a high energy
- 4 resonance, shown as black and red vertical dashed lines in the plots in Fig. 2. For each resonance,
- 5 further visualization of the transition energies is enabled by plots of the moduli of the PR
- 6 resonances, ²³ shown as grey dashed lines in Fig. 2:

7
$$\Delta \rho(E) = \frac{|C|}{[(E-E_0)^2 + \Gamma^2]^{\frac{m}{2}}}$$
 (3)

- 8 With increasing N fraction and/or Bi fraction, there is a monotonic decrease, i.e. a redshift, of the
- 9 bandgap to lower energies. For some spectra, a second resonance is apparent at slightly higher
- 10 energy than the bandgap, likely due to strain-induced splitting of the light-hole and heavy-hole
- bands. 23 For other spectra, the broadening of the PR resonances and the small degree of splitting
- makes it difficult to resolve the second transition. In all cases, the bandgap energy, Eg, is
- determined as the sum of the excitonic transition (determined from the low-energy PR resonance)
- 14 plus the exciton binding energy (~8meV), taking into account strain-induced shifts of the band-
- 15 edges at the measurement temperature (\sim 20K).
- In Fig. 3, contours of bandgap and out-of-plane misfit are presented on a plot of Bi vs. N
- mole fractions for GaAs_{1-x-y}N_xBi_y films. Dashed black lines indicate contours of constant out-of-
- 18 plane misfit, while circular and square symbols represent individual GaAsNBi films, as described
- 19 for Fig. 1. Bandgaps measured by PR for specific films are labeled beside each data point. Solid
- 20 contours indicate the composition-dependence of the bandgap energy (in eV), E_{GaAsNBi}, determined
- 21 by fitting the measured bandgaps and compositions using the parameterization scheme of Tixier
- 22 et al.:²¹

$$E_{GaAsNBi}(x_N, y_{Bi}) = E_{GaAs} - \Delta_N(x_N) - \Delta_{Bi}(y_{Bi}) - A\Delta_N(x_N)\Delta_{Bi}(y_{Bi})$$
(4)

6

- where E_{GaAs} is the bandgap of GaAs at 20 K, $\Delta_N(x_N)$ is the N-induced bandgap reduction in
- 2 GaAsN, $\Delta_{Ri}(y_{Ri})$ is the Bi-induced bandgap reduction in GaAsBi, and A is an adjustable N-Bi
- 3 coupling parameter. The N-induced bandgap reduction (in eV) is expressed as:

$$\Delta_N(x_N) = x_N (E_{GaAS} - E_{GaN}) + b_{GaASN} x_N (1 - x_N)$$
 (5)

- where E_{GaN} is the bandgap of GaN and b_{GaAsN} is the bowing parameter (in eV) with a double-
- 6 exponential dependence on N fraction:^{24,25}

$$b_{GaASN}(x_N) = 9.4 + 23.8e^{-x_N/0.0038} + 11.9e^{-x_N/0.028}$$
 (6)

- 8 The double-exponential dependence of the bowing parameter on x_N has been attributed to three
- 9 regimes of bandgap energy, which are dominated by single-impurity N levels, N pair and cluster
- states, and alloy behavior, respectively. ^{25,26,27} To estimate the Bi-induced bandgap reduction, we
- used our PR determination of the GaAsBi bandgap as $\Delta_{Bi}(y_{Bi}) = 7.3y_{Bi}$ (in eV), which is similar
- to the average value $7.8y_{Bi}$ from earlier reports. ^{19,28,29,30,31} Using a non-linear least-squares fit to
- Eqn. (4), 32,33 the N-Bi coupling parameter $A = -0.02 \pm 0.10$ eV⁻¹, which corresponds to a value of
- -(1-2) meV for the final term in Eqn. (4). Thus, the quaternary bandgap reduction is essentially the
- 15 sum of the individual bandgap reductions, suggesting that N and Bi independently influence the
- band edges, as predicted by Broderick et al., but in contrast to earlier reports that indicate non-
- zero values of A, 1,21 which correspond to additional bandgap reductions of <20 meV and <100
- 18 meV.21
- We next examine PL spectra for a selection of GaAs_{1-x-y}N_xBi_y films with PR spectra shown
- in Fig. 2. In Fig. 4(a), PL spectra for a film with $x_N = 0.007$ and $y_{Bi} = 0.034$ are plotted for
- 21 measurement temperatures ranging from 7 K to 125 K. With increasing measurement temperature,
- 22 the PL peak energy decreases monotonically. In addition, above 120K, the PL intensity decreases,
- and the emission line-shape is asymmetric with an extended low-energy tail, ^{34,35} often associated

11

12

13

14

15

16

17

18

19

20

21

22

2 temperatures lower than those for the GaAs host. However, the narrow PR resonances and VB

3 splitting into heavy and light hole bands suggest high quality, homogeneous alloy films. In Fig.

4 4(b), the PL peak energies as a function of measurement temperature are compared with the

5 bandgap energy of the film determined from PR measurements collected at 20 K. A solid black

6 line shows a projection of the bandgap to high temperatures using the Varshni model, ³⁶

7
$$E(T) = E(0) - \frac{\alpha T^2}{(T+\beta)}$$
 (7)

8 using the parameters for GaAs ($\alpha = 5.41 \times 10^{-4} \text{ meV/K}$, $\beta = 204 \text{ K}$). The ~160 meV difference

9 between the PR-determined bandgap, E_{PR} , and the PL-determined energy gap, E_{PL} , i.e. the Stokes

shift, suggests emission from localized states.

To examine the origins of the localized state emission, in Fig. 5, we consider PL spectra for several films from (a) the N flux series and (b) the Bi flux series. For all Bi-containing films, the Stokes shifts range from 0.15 to 0.18 eV. In contrast, for GaAsN films (i.e. $y_{Bi} = 0$) in Figs. 5(b) and S1, the differences between E_{PL} and E_{PR} are < 60 meV. Taken together, these results suggest that the 7 K PL emission is dominated by an optical transition involving a Bi-related state within the bandgap, approximately 0.18 eV above the valence band edge. Interestingly, Janotti et al. predicted a Bi-induced isovalent defect level at 0.18 eV above the valence band edge of GaAsNBi. Further work is needed to resolve the atomistic origins of the Bi-related states.

In summary, we have examined the alloy composition-dependence of the energy bandgap and lattice misfit in GaAsNBi alloys. Using direct measurements of N and Bi mole fractions and out-of-plane misfit, we identify a N to Bi mole fraction ratio of 0.83 for lattice-matching to GaAs. Using the substitutional N mole fraction, without including the interstitial N, the lattice-matched

N to Bi mole fraction ratio becomes 0.61, in agreement with the predictions of Janotti et al. In

PLEASE CITE THIS ARTICLE AS DOI: 10.1063/1.5057424

addition, a comparison of photoreflectance and photoluminescence measurements suggests the presence of Bi-related states ~0.18 eV above the valence band edge. These findings offer a predictive guide for bandgap engineering using GaAsNBi alloys and provide insight into the combined influence of Bi and N on electronic structure that is likely to extend to other emerging dilute nitride-bismide alloys, such as GaPNBi and InAsNBi.

7

9

10

11

1

2

3

4

5

6

SUPPLEMENTAL MATERIALS

See the supplemental materials for details of our x-ray rocking curve analysis to determine in-plane strain and its impact on the conduction and valence band edges. In addition, tabulated values of strain and other parameters used to fit the photoreflectance (PR) spectra, as well as PR spectra for the 400 nm thick films, are included.

12 13

14

ACKNOWLEDGEMENTS

15 We gratefully acknowledge support from the National Science Foundation (Grant Nos. 16 DMR 1410282 and DMR 1810280) and the U.S. Department of Energy Office of Science 17 Graduate Student Research (SCGSR) Program. Partial support is also provided by the Center for 18 Integrated Nanotechnologies (CINT), a DOE nanoscience user facility jointly operated by Los 19 Alamos and Sandia National Laboratories. W. M. Linhart acknowledges support from the Polish 20 National Science Center (NCN) grant No. 2014/13/D/ST3/01947. This work was partly supported 21 by a grant from the Ministry of Research and Innovation, CNCS-UEFISCDI, project number PN-III-P4-ID-PCE-2016-0742, within PNCDI III. 22

2

1

FIGURE CAPTIONS

3 FIG. 1: Contours of out-of-plane misfit, ε_{\perp} , presented on a plot of bismuth mole fraction, y_{Bi} , and 4 nitrogen mole fraction, x_N, for GaAs_{1-x-y}N_xBi_y films; circular and square symbols correspond to 5 100 nm and 400 nm thick films, respectively. The percent out-of-plane misfit, ϵ_{\perp} , determined from 6 (004) XRC, is labeled adjacent to each point. Dashed black lines represent contours of constant 7 misfit, determined with a planar fit to the data points, indicating lattice-matching for a N to Bi 8 mole fraction ratio of 0.83. Lattice-matched N to Bi mole fraction ratios of 0.59 computed by 9 Janotti et al., and 0.49 estimated from x-ray diffraction determinations of N mole fraction by 10 Huang et al.¹⁹ are shown by gray lines. Cross symbols represent GaAsNBi films from Ref. 21. The 11 uncertainty in the ϵ_{\perp} contour lines is \pm 0.04%, defined as the standard deviation between the fit and 12 measured values of ϵ_{\perp} . 13 14 FIG. 2: Photoreflectance (PR) spectra collected at 20 K from 100 nm thick GaAs_{1-x-v}N_xBi_v films, 15 with corresponding N and Bi mole fractions, x_N and y_{Bi}, displayed above each spectrum for (a) the 16 N flux series and (b) the Bi flux series. For each spectrum, a PR resonance attributed to the bandgap 17

with corresponding N and Bi mole fractions, x_N and y_{Bi} , displayed above each spectrum for (a) the N flux series and (b) the Bi flux series. For each spectrum, a PR resonance attributed to the bandgap energy, E_g , is indicated by a black dashed line. With increasing x_N and/or y_{Bi} , the E_g values decrease monotonically. For some spectra, a second transition, attributed to strain-induced splitting of the light-hole and heavy-hole bands, is indicated by a red vertical dashed line. The energy of each resonance was determined by fitting each spectrum with the Aspnes formula²² (solid lines). The moduli of the PR resonances are shown as gray dashed lines below each PR

22 spectrum.

18

19

20

21

23

10

 $2 \quad \text{bismuth mole fraction, } y_{Bi}\text{, and nitrogen mole fraction, } x_N\text{, for } GaAs_{1\text{-}x\text{-}y}N_xBi_y \text{ films. } Values \text{ of } E_g$

3 determined from photoreflectance spectra collected at 20 K are labeled adjacent to each point.

4 Solid lines of constant E_g were determined by a non-linear least-squares fit of Eqn. (4) to the data

5 points. Dashed lines of constant ε_{\perp} , were determined as described for Fig. 1, with lattice-matching

6 to GaAs at a N to Bi mole fraction ratio of 0.83. The uncertainty in the E_g contour lines is \pm 14

7 meV, defined as the standard deviation between the fit and the measured values of E_g.

8

9 FIG. 4: (a) Photoluminescence spectra collected from a GaAs_{0.959}N_{0.007}Bi_{0.034} film at measurement

10 temperatures ranging from 7 to 125 K. The N and Bi mole fractions are listed as x_N and y_{Bi} . With

11 increasing measurement temperature, the PL peak energy decreases monotonically. (b) PL peak

12 energy versus measurement temperature, compared to photoreflectance (PR)-determined bandgap

13 energy, Eg, at 20 K. A solid black line shows a projection of the Eg to high temperatures using the

14 Varshni model³⁶ with the parameters for GaAs.³⁷

15

16 FIG. 5: Photoluminescence (PL) spectra collected at 7 K for selected GaAs_{1-x-y}N_xBi_y films whose

17 photoreflectance spectra were shown in Fig. 2. A comparison of the PL-determined peak energies,

18 E_{PL}, with the PR-determined bandgap energies, E_{PR}, in Fig. 2 reveals similar values for the GaAsN

19 film. For the GaAsNBi films, the difference between E_{PR} and E_{PL}, i.e. the Stokes shift, ranges from

20 0.15 to 0.18 eV, likely due to Bi-related states within the bandgap.

¹ A. Janotti, S.-H. Wei, and S.B. Zhang, Phys. Rev. B 65, 115203 (2002).

² S.J. Sweeney and S.R. Jin, J. Appl. Phys. 113, 043110 (2013).

³ J. Occena, T. Jen, E.E. Rizzi, T.M. Johnson, J. Horwath, Y.Q. Wang, and R.S. Goldman, Appl. Phys. Lett. 110, 242102 (2017).

⁴ Y. Zhang, A. Mascarenhas, and L.-W. Wang, Phys. Rev. B 71, 155201 (2005).

⁵ S. Francoeur, S. Tixier, E. Young, T. Tiedje, and A. Mascarenhas, Phys. Rev. B 77, 085209 (2008).

⁶ K. Alberi, O.D. Dubon, W. Walukiewicz, K.M. Yu, K. Bertulis, and A. Krotkus, Appl. Phys. Lett. 91, 051909 (2007).

⁷ C.A. Broderick, M. Usman, and E.P. O'Reilly, Semicon. Sci. Tech. 28, 125025 (2013).

⁸ C.-Z. Zhao, H.-Y. Ren, T. Wei, S.-S. Wang, and K.-Q. Lu, J. Electron. Mat. 47, 4539 (2018).

⁹ V. Virkkala, V. Havu, F. Tuomisto, and M.J. Puska, Phys. Rev. B 88, 235201 (2013).

¹⁰ J. Occena, T. Jen, H. Lu, B.A. Carter, T.S. Jimson, A.G. Norman, and R.S. Goldman, Appl. Phys. Lett. 113, 211602 (2018).

¹¹ R.S. Goldman, H.H. Wieder, and K.L. Kavanagh, Appl. Phys. Lett. 67, 344 (1995).

¹² J.W. Matthews and A.E. Blakeslee, J. Crystal Growth 27, 118 (1974).

¹³ R. People and J.C. Bean, Appl. Phys. Lett. 47, 322 (1985).

¹⁴ P.M.J. Maree, J.C. Barbour, J.F. Van der Veen, K.L. Kavanagh, C.W.T. Bulle-Lieuwma, and M.P.A. Viegers, J. Appl. Phys. 62, 4413 (1987).

¹⁵ R.S. Goldman, K.L. Kavanagh, H.H. Wieder, S.N. Ehrlich, and R.M. Feenstra, J. Appl. Phys. 83, 5137 (1998).

¹⁶ M. Reason, X. Weng, W. Ye, D. Dettling, S. Hanson, G. Obeidi, and R.S. Goldman, J. Appl. Phys. 97, 103523 (2005).

¹⁷ T. Jen, G. Vardar, Y.Q. Wang, and R.S. Goldman, Appl. Phys. Lett. 107, 221904 (2015).

¹⁸ M. Reason, H.A. McKay, W. Ye, S. Hanson, R.S. Goldman, and V. Rotberg, Appl. Phys. Lett. 85, 1692 (2004).

¹⁹ W. Huang, K. Oe, G. Feng, and M. Yoshimoto, J. Appl. Phys. 98, 053505 (2005).

²⁰ P. Wei, S. Tixier, M. Chicoine, S. Francoeur, A. Mascarenhas, T. Tiedje, and F. Schiettekatte, Nucl. Instrum. Meth. B 219–220, 671 (2004).

²¹ S. Tixier, S.E. Webster, E.C. Young, T. Tiedje, S. Francoeur, A. Mascarenhas, P. Wei, and F. Schiettekatte, Appl. Phys. Lett. 86, 112113 (2005).

²² D.E. Aspnes, Surf. Sci. 37, 418 (1973).

²³ R. Kudrawiec and J. Misiewicz, in *Semiconductor Research*, edited by A. Patane and N. Balkan (Springer Berlin Heidelberg, Berlin, Heidelberg, 2012), pp. 95–124.

²⁴ M. Reason, Ph.D. Thesis, University of Michigan, 2006, p. 140.

²⁵ U. Tisch, E. Finkman, and J. Salzman, Appl. Phys. Lett. 81, 463 (2002).

²⁶ P.R.C. Kent and A. Zunger, Phys. Rev. B 64, 115208 (2001).

²⁷ R.L. Field, Y. Jin, H. Cheng, T. Dannecker, R. Jock, Y. Wang, C. Kurdak, and R.S. Goldman, Phys. Rev. B 87, 155303 (2013).

²⁸ S. Tixier, M. Adamcyk, T. Tiedje, S. Francoeur, A. Mascarenhas, P. Wei, and F. Schiettekatte, Appl. Phys. Lett. 82, 2245 (2003).

²⁹ S. Francoeur, M.J. Seong, A. Mascarenhas, S. Tixier, M. Adamcyk, and T. Tiedje, Appl. Phys. Lett. 82, 3874 (2003).

³⁰ K. Alberi, O.D. Dubon, W. Walukiewicz, K.M. Yu, K. Bertulis, and A. Krotkus, Appl. Phys. Lett. 91, 051909 (2007).

³¹ A.R. Mohmad, F. Bastiman, J.S. Ng, S.J. Sweeney, and J.P.R. David, Phys. Status Solidi C 9, 259 (2012).



 $^{^{\}rm 32}$ K. Levenberg, Quart. Appl. Math. 2, 164 (1944).

³³ D. Marquardt, J. Soc. Ind. Appl. Math. 11, 431 (1963).

³⁴ S. Imhof, A. Thränhardt, A. Chernikov, M. Koch, N.S. Köster, K. Kolata, S. Chatterjee, S.W. Koch, X. Lu, S.R. Johnson, D.A. Beaton, T. Tiedje, and O. Rubel, Appl. Phys. Lett. 96, 131115 (2010).

³⁵ T. Wilson, N.P. Hylton, Y. Harada, P. Pearce, D. Alonso-Álvarez, A. Mellor, R.D. Richards, J.P.R. David, and N.J. Ekins-Daukes, Sci. Rep. 8, 6457 (2018).

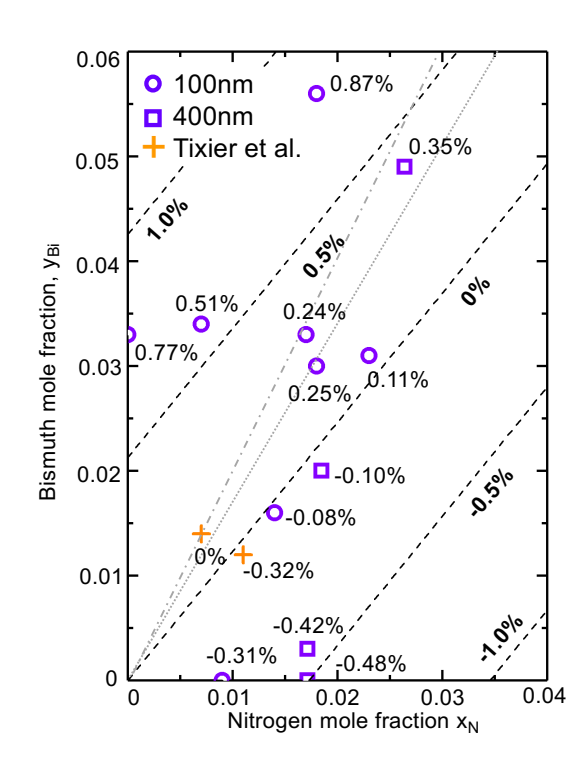
³⁶ Y.P. Varshni, Physica 34, 149 (1967).

³⁷ I. Vurgaftman, J.R. Meyer, and L.R. Ram-Mohan, J. Appl. Phys. 89, 5815 (2001).

AIP Publishing

Applied Physics Letters

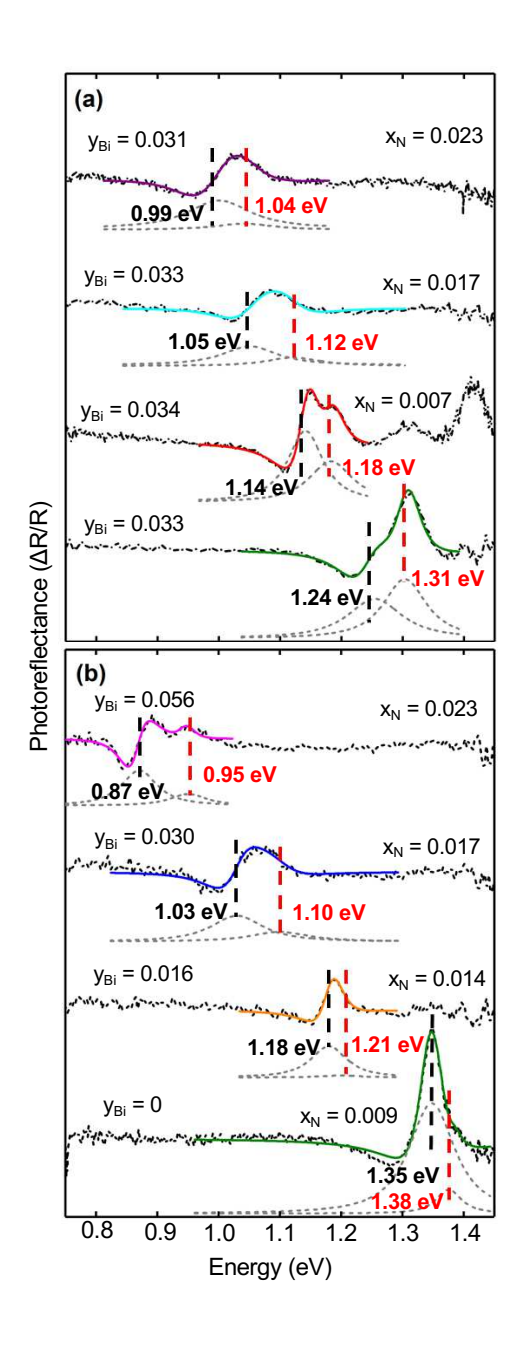
This is the author's peer reviewed, accepted manuscript. However, the online version of record will be different from this version once it has been copyedited and typeset.



AP Publishing

Applied Physics Letters

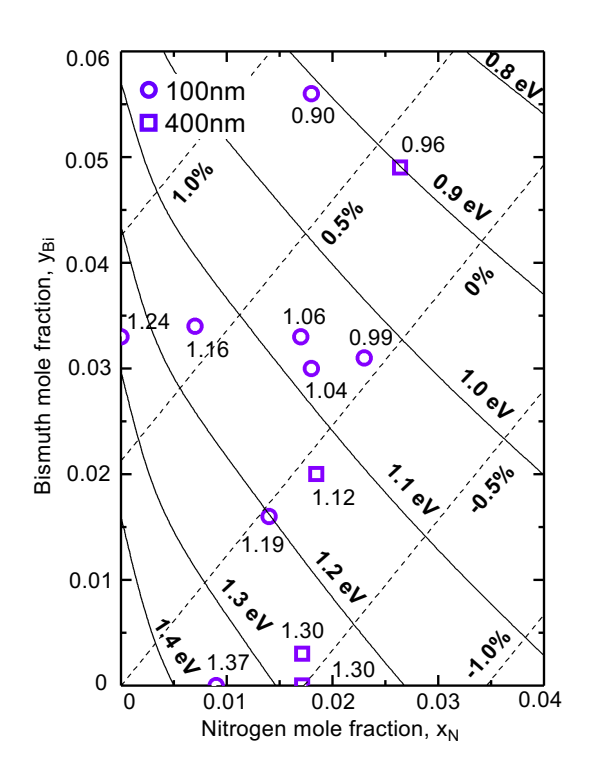
This is the author's peer reviewed, accepted manuscript. However, the online version of record will be different from this version once it has been copyedited and typeset.



AP Publishing

Applied Physics Letters

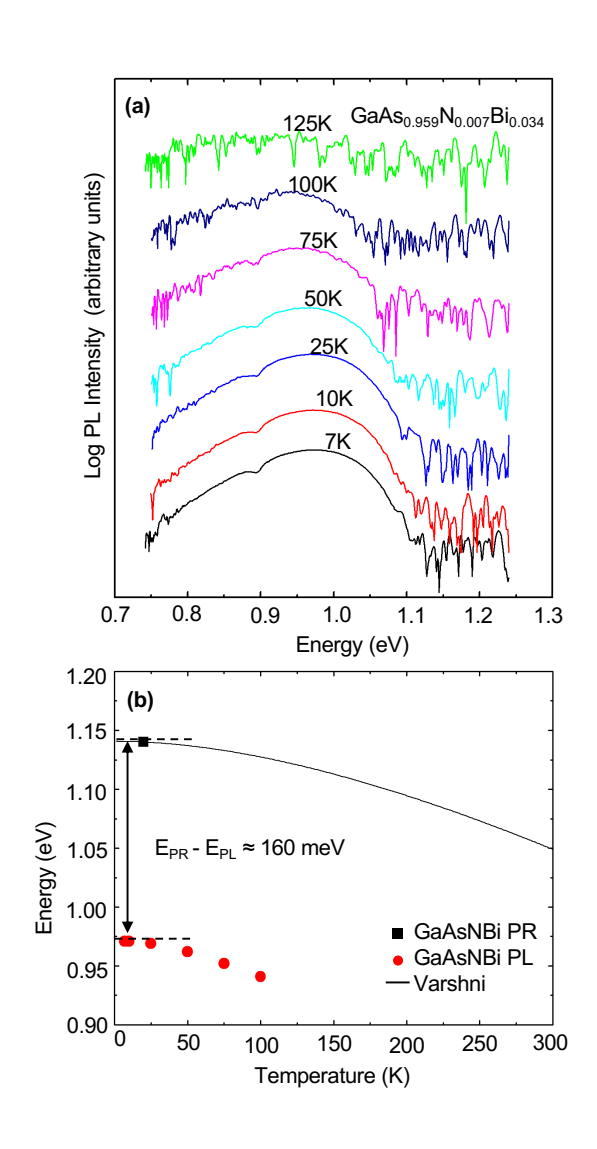
This is the author's peer reviewed, accepted manuscript. However, the online version of record will be different from this version once it has been copyedited and typeset.



AIP

Applied Physics Letters

This is the author's peer reviewed, accepted manuscript. However, the online version of record will be different from this version once it has been copyedited and typeset.



AIP Publishing

Applied Physics Letters

This is the author's peer reviewed, accepted manuscript. However, the online version of record will be different from this version once it has been copyedited and typeset.

